Title

Breaking OER and CER scaling relations via strain and its relaxation in RuO₂ (101)

Author Names and affiliations

Prajwal Adiga¹, William Nunn², Cindy Wong¹, Anusha K. Manjeshwar², Sreejith Nair², Bharat Jalan^{2,*}, Kelsey A. Stoerzinger^{1,3,*}

- ¹ School of Chemical, Biological and Environmental Engineering, Oregon State University, Corvallis, Oregon, 97331, USA
- ² Department of Chemical Engineering and Materials Science, University of Minnesota, Minneapolis, Minnesota 55455, USA
- ³ Physical Sciences Division, Pacific Northwest National Laboratory, Richland, Washington, 99254, USA

Corresponding author

* Email address: <u>bjalan@umn.edu</u>, <u>kelsey.stoerzinger@oregonstate.edu</u>

Abstract

Green hydrogen production from abundant water sources is an important component of renewable energy storage. Water oxidation catalysts are typically considered bound by adsorbate scaling relations, limiting their activity for the oxygen evolution reaction (OER) as well as selectivity between OER and the chlorine evolution reaction (CER) that compete in saline water streams. RuO₂ is highly active for both reactions, and recent measurements have shown the OER activity is greater on undercoordinated, high index facets compared to the lowest-energy (110) facet often studied. The growth of such orientations as epitaxial films, however, can result in appreciable strain and potential surface faceting via its relaxation. We find the activity and selectivity towards OER and CER vary with thickness in epitaxial (101) RuO₂ thin films: OER activity decreases 4x as film thickness increases from 8 nm to 48 nm, while CER activity is comparable. Thus, strain and its relaxation can be used to break scaling relationships between OER and CER, highlighting the important role that defects play in selective oxidation processes on RuO₂ in chloride-containing media.

Keywords

strain, defects, oxygen evolution reaction, chlorine evolution reaction, epitaxial thin films

1. Introduction

The slow kinetics of the oxygen evolution reaction (OER) requires efficient catalysts to enable green hydrogen generation via electrolysis of abundant water sources ^{1,2}. Rutile IrO₂ and RuO₂ are exceptionally active OER catalysts ³⁻⁶, and also demonstrate high activity for the chlorine evolution reaction (CER) that competes with the OER during the electrolysis of saline water ⁷. Similarly, OER is a parasitic reaction during the chlor-alkali process ^{8,9}. OER is a four-electron transfer process involving multiple intermediates, namely *O, *OH and *OOH ¹⁰. On the (110) rutile surface ^{11,12}, the binding energies of these OER intermediates scale linearly with one

another due to the common binding of an O atom to the same active (metal) site ^{5,13,14}. Thus, Man et al. introduced the binding energy difference of *OH and *O as a universal descriptor for oxygen evolution activity ⁵. These scaling relationships also fundamentally limit OER activity, as affinity for any given adsorbate cannot be manipulated independently, constraining the performance of any electrocatalyst to a minimum theoretical overpotential of 0.37 V ¹⁵. Similarly, the CER on these surfaces proceed through intermediates (i.e. *OCI) whose binding energies also scale with those of the OER ¹⁶, prohibiting independent tuning of the reaction rates and therefore catalyst selectivity.

Adsorbate scaling relations may be circumvented in active sites with unique geometries, such as those involving adsorbate H-bonding ¹⁷. Calculations suggest such active sites might be induced via doping at the neighboring bridge site on RuO₂ (110) ¹⁷, although more recent calculations suggest H-bonding at the bridge site may be involved in the OER mechanism in the absence of doping as well ¹⁸. Defects on RuO₂ (110) can increase OER activity via strengthening binding to oxygen ^{19,20}, but their presence on both low and high index facets has been predicted to change the reaction mechanism ²¹ and catalyst stability ²² as well. Specifically, defects may trigger a switch from the scaling-bound adsorbate evolution mechanism (AEM) to the lattice oxygen evolution mechanism (LOEM), typically observed to be pH-dependent ^{23,24}. Experimentally, oriented IrO₂ and RuO₂ exhibit greater OER activity on higher index facets ^{25,26}, related to the computed strength of *O binding but possibly also influenced by active site geometry. Theoretical study ²⁷ of RuO₂ has also suggested the CER/OER selectivity may be facet-dependent, perhaps suggesting unique scaling between reaction intermediates.

Strain offers an opportunity to break scaling relations in catalysis ²⁸. Differences in adsorbate binding can arise via changes in electronic structure ^{29,30}, and strain relaxation can induce defects ^{31,32} and surface faceting ³³ with subsequent impact on activity as well. In high surface area systems, strain can be introduced by selective leaching in alloys ³⁴ and generation of coreshell particles ^{35,36}. Given the experimental challenges in controlling and characterizing such systems ³⁷, we take a more fundamental approach ³⁸, where strain can be systematically introduced via epitaxial growth on different substrates ^{39,40} or changing film thickness ^{41,42}.

Here we consider the (101) orientation of RuO_2 , more active for OER than the low-index (110) facet ⁴³, incorporating defects via strain relaxation in epitaxial thin films. While the thinnest films (< 10 nm) exhibit a high degree of strain ³³, large lattice mismatch with an r- Al_2O_3 or TiO_2 substrate introduces defects upon strain relaxation in thicker films. This relaxation appears to influence the *O binding of surface sites, with thicker films ~4x less active at 1.55 V_{RHE} . While defects have a dramatic impact on OER, the activity in a Cl-containing acidic electrolyte suggests that such defects have minimal effect on CER activity. These findings support that strain and its relaxation can control both activity and selectivity in oxidation reactions.

2. Experimental section

2.1 RuO₂ film growth and characterization

High quality RuO₂ films were grown using the solid-source metal–organic molecular beam epitaxy (SS-MOMBE) technique ⁴⁴, with Ru(acac)₃ (97%, Millipore Sigma) sublimed from an effusion cell (E-Science, Inc.) at a temperature of 100°C. Using a radio-frequency inductively coupled oxygen plasma source (Mantis Inc.), atomic oxygen was supplied with an oxygen background pressure of ~5×10⁻⁶ Torr. Films were grown on r-plane sapphire (*r*-Al₂O₃) and TiO₂ substrates (MTI Corporation) at a substrate temperature of 300°C. Film growth was monitored before, during and after growth using reflection high-energy electron diffraction (RHEED, Staib Instruments). Surface roughness was measured using atomic force microscopy (AFM, Bruker) post growth. Structural characterization was carried out using high-resolution X-ray diffraction (HRXRD, Rigaku SmartLab XE), and reciprocal space mapping (RSM). Thickness was determined using grazing incidence x-ray reflectivity (GIXR). Temperature dependent four-probe resistivity measurements were performed in the Van der Pauw geometry (Quantum Design DynaCool Physical Property Measurement System). As shown in Figure S1, the films have atomically-smooth terraces from AFM and changes in strain with film thickness are evident by the observed shift in RuO₂ (101) peaks from HRXRD.

2.2 Experimental testing procedure

Electrochemical measurements ³⁸ were conducted with a VSP-300 Biologic® potentiostat at room temperature and ambient pressure. A standard three-electrode setup was comprised of a RuO₂ working electrode, a Pt counter and Ag/AgCl reference electrode in a glass Pine® cell. The RuO₂ film was affixed to a glassy carbon electrode with double-sided copper tape, electrically contacting one edge of the RuO₂ film. Kapton tape defined a circular area of RuO₂ exposed to the electrolyte 38 rotated at a constant rate of 900 RPM using a Pine® modulated speed rotator. Electrolytes were prepared with 18.2 MΩ-cm Millipore water, using KOH (Sigma-Aldrich, Semiconductor gr.), H₂SO₄ (Fisher Scientific, ACS gr.), and KCl (Macron, ACS gr.) as noted. Potentio-electrical impedance spectroscopy (PEIS) was performed at the open circuit potential (OCP) with an amplitude of 10 mV. Potentials were corrected for the electrolyte/cell resistance from the high frequency intercept of the real impedance. Discrete points on the Tafel plot were obtained from chronoamperometry holding each potential for 5 min (Figure S2). OER measurements in KOH were carried out in O₂-saturated (Airgas, UHP gr.) electrolyte to fix the equilibrium potential. For comparing OER activity across pH, the concentration of KOH was varied from 0.01 M KOH, 0.1 M KOH, and 1 M KOH. For measurements comparing OER and CER in 0.1 M H₂SO₄, the electrolyte was saturated with N₂. For assessment of charge transfer, 5 mM of K₄Fe(CN)₆-3H₂O (Sigma-Aldrich, ACS gr.) and 5 mM of K₃Fe(CN)₆ (Merck, ACS gr.) were added to Ar-saturated (Airgas, ultrahigh-grade purity) 0.1 M KOH.

3. Results and discussion

We first consider RuO_2 grown on TiO_2 substrates of different orientations by SS-MOMBE ³³. As seen previously in literature for epitaxial RuO_2 grown at higher temperatures by pulsed laser deposition (PLD) ^{3,25}, we find that the higher surface energy facets ^{25,45} are more active than the lowest energy (110) facet for OER (Figure S3), with the (101) facet showing the highest activity.

We next consider RuO_2 (101) films of different thicknesses grown on r- Al_2O_3 (RuO_2/r - Al_2O_3) using SS-MOMBE, where RuO_2 (101) mismatch with r- Al_2O_3 is greater than its mismatch with TiO_2 (101), exacerbating relaxation-induced effects 33 . The resulting films showed a single (101) orientation by XRD and a smooth surface by AFM (Figure S1). Four-point probe measurements show resistivity decreases with increasing film thickness but is sufficiently low for good metallic electron transport 33 , with similar metallic-like charge-transfer properties measured in situ via a fast-redox couple (Figure S4(b)). In comparing films from 8 to 48 nm, the increase in full width at half maximum (FWHM) of the rocking curve of the RuO_2 (101) peak suggests a consistent relaxation of strain with increasing film thickness 33 .

3.1 Thickness- and substrate-dependent OER

Figure 1(a) (and figure S5(a)) shows OER cyclic voltammetry (CV) for RuO_2 (101)/r- Al_2O_3 , where activity decreased with increasing RuO_2 film thicknesses, further supported by chronoamperometry (CA) (Figure 1(b), S5(b)). The difference in activity is similar in magnitude to that observed comparing different crystallographic orientations (Figure S3), suggesting strain relaxation via defect formation and/or faceting has an appreciable effect on OER activity.

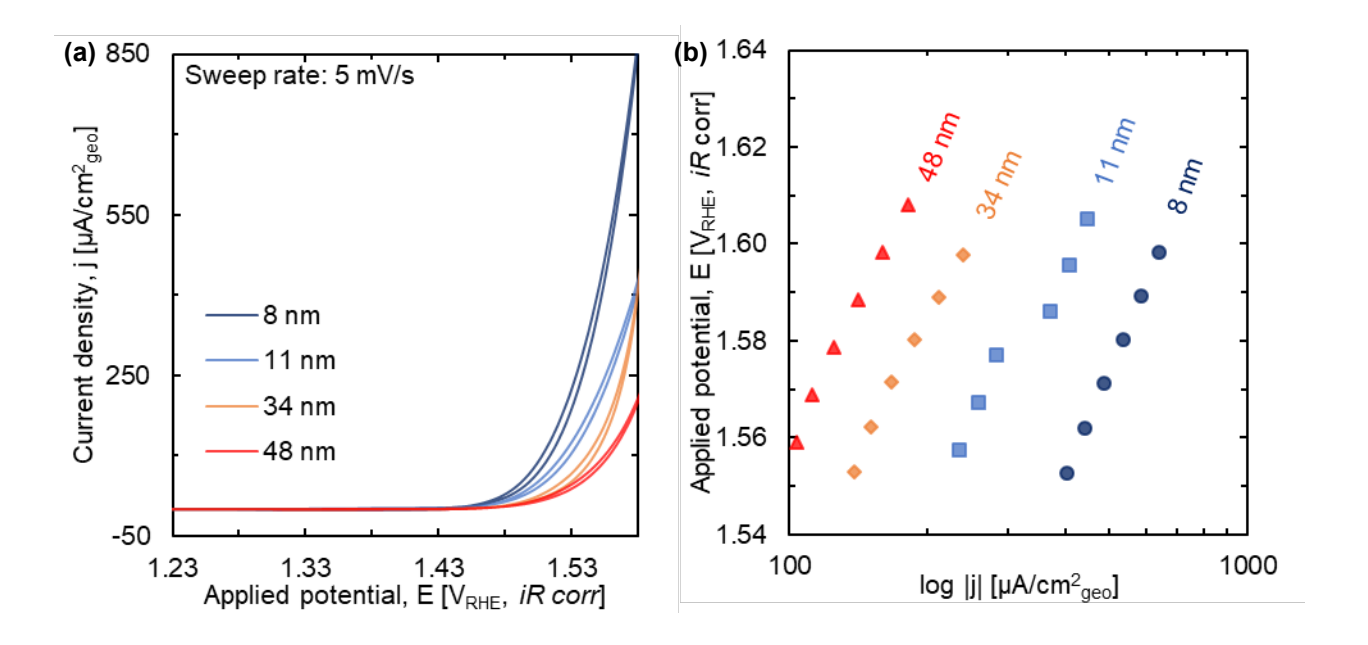


Figure 1: Electrochemical measurements on RuO₂ (101)/*r*-Al₂O₃ films in O₂-saturated 0.1 M KOH show activity decreases with increasing thickness, both by (a) CV at 5 mV/s and (b) CA (Figure S2), presented as a Tafel plot.

To better understand the origins of thickness impacting OER on RuO₂, we experimentally assessed the strength of *OH and *O binding via electroadsorption. Calculations in literature

attribute Ru redox behavior to charge transfer from the electroadsorption of OH (* $H_2O \rightarrow *OH + H^+ + e^-$, ~1 V vs RHE) and O (* $OH \rightarrow *O + H^+ + e^-$, ~1.4 V vs RHE) 26,46 . Considering different RuO₂ orientations grown on TiO₂, we see that *O forms at higher applied potentials on the more active (101) facet (Figure 2a), consistent with the calculated higher *O binding energy for this orientation compared to the (110) facet 25,26 . However, this feature is broader in comparison to the (110) facet, suggesting that a range of local environments might be available on the catalyst surface. Considering the lattice mismatch between (101) RuO₂ and (101) TiO₂ (-1.8% a-axis, +3.0% c-axis), such variation could arise from residual strain or its relaxation via defect formation or faceting. Scanning transmission electron microscopy (STEM) images of the (101) orientation 33 showed no misfit dislocations at the substrate/film interface and an out of plane lattice parameter consistent with strained growth on a TiO₂ substrate, but faceting with the (111) termination along the [$\bar{1}01$] direction was apparent. This suggests that (101) RuO₂ exhibits strain relaxation accompanying surface faceting.

Surprisingly, the singular broad *O feature for RuO₂ (101) grown on TiO₂ is resolved into two well-defined peaks on *r*-Al₂O₃ grown RuO₂ (101), where greater mismatch may exacerbate relaxation-induced effects. Subtle changes in *O electroadsorption are then observed with changing RuO₂ film thickness on *r*-Al₂O₃, as shown in Figure 2(b). Weighting between *O features at ~1.35 V and ~1.40 V shifts to stronger electroadsorption with increasing film thicknesses, consistent with calculations in literature showing increased *O binding with defect formation ¹⁹. For the thicker films, higher order Ru oxidation at ~1.5 V is resolved as reduced OER activity no longer yields overlap in current response between these processes. In contrast, the *OH electroadsorption feature remains broad without notable changes as film thickness increases (Figure S7). Distinctive changes in *O and *OH adsorbate binding (Figure S7), retaining similar charge (Figure S8) are surprising given typical scaling relations ⁵, and may indicate unique coordination environments on the surface.

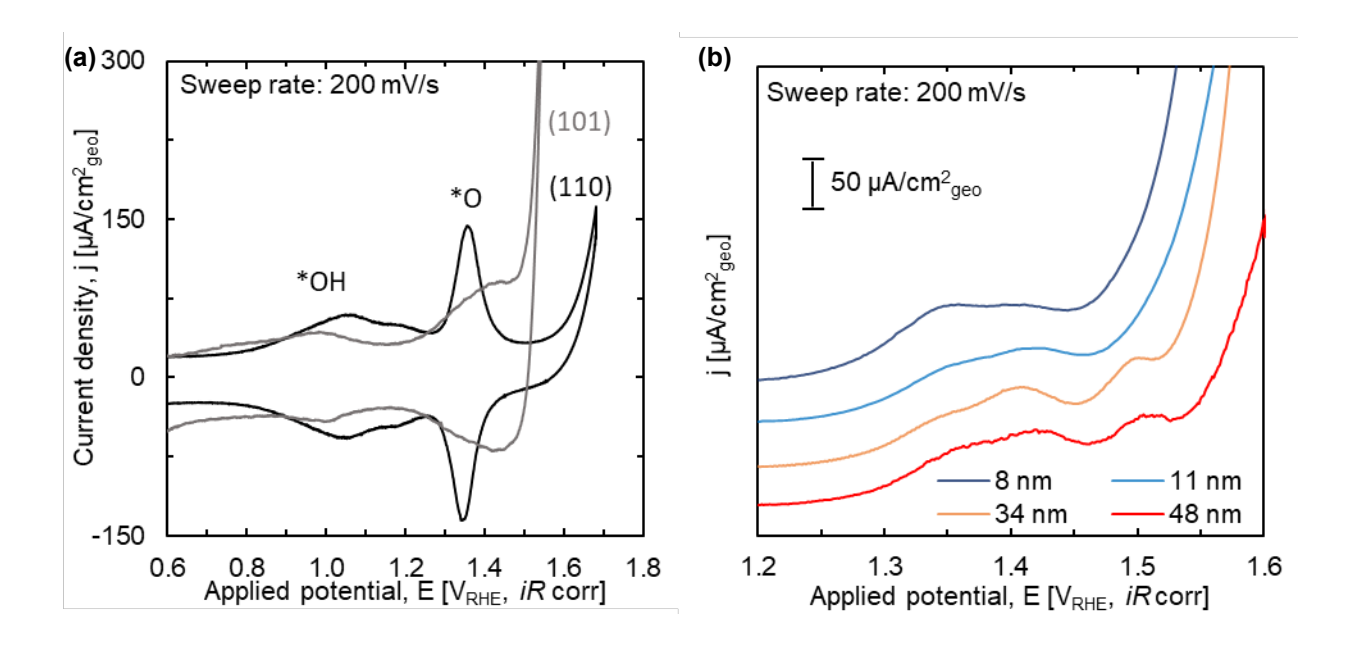


Figure 2: Ru surface redox feature comparison for RuO_2 in N_2 saturated 0.1 M KOH. (a) CV of (101)- and (110)-oriented RuO_2 films (~10 nm) grown on TiO_2 substrates with well-defined

features for *OH and *O electroadsorption and OER activity that differ greatly with crystallographic orientation. (b) Linear sweep voltammetry (LSV) of RuO₂ (101)/*r*-Al₂O₃ films with different thicknesses shows *O shifting to higher oxidative potential with increasing film thickness offset for clarity.

To better disentangle the effects of strain and its relaxation, we compared ~10 nm thick RuO₂ (101) grown on TiO₂ (101) and r-Al₂O₃. While the d-spacing for such films is similar at this thickness, the larger lattice mismatch with r-Al₂O₃ leads to greater defect formation, likely evident from the lack of lattice fringes in XRD (Figure S9). The OER activity is indeed lower for RuO₂ (101) grown on r-Al₂O₃ relative to TiO₂ (101), consistent with defect formation and/or faceting resulting in lower OER activity.

3.2 Potential changes in OER mechanism

We next assess whether RuO₂ relaxation via defect or facet formation might also lead to changes in OER mechanism, assessed here by the pH dependence of activity. In previous consideration of ~25 nm (101)- and (111)-oriented RuO₂ grown by PLD on TiO₂, online electrochemical mass spectroscopy (OLEMS) measurements did not observe ¹⁸O exchange with the lattice on the timescale of measurements, indicating OER proceeded via the AEM mechanism on a wide range of RuO₂ facets ²⁵. However, both orientations exhibited pHdependent OER ⁴⁷, attributed to the super-Nernstian shift in Ru redox ⁴⁸. In contrast, calculations by Zagalskaya et al. reported that the lattice oxygen evolution mechanism (LOEM) may be competitive at defect sites on RuO₂ (such as metal vacancies) ²¹. The rate of LOEM typically increases with solution pH, in contrast to the AEM which is generally considered pHindependent ²³. Similar to previous measurements on ~25 nm (101) RuO₂ films ⁴⁸, we also observe that activity at 1.6 V vs RHE increases with pH for the thickest (48 nm) film (Figure S4(a)), however the thinnest (8 nm) RuO₂ film shows nominally pH-independent OER, where pH-independent OER activity has also been observed on particles ⁴⁹. Thus, strain relaxation may lead to mechanistic changes via triggering lattice oxygen involvement or modifying pHdependent Ru redox, of interest for future studies via ¹⁸O labeling.

3.3 Breaking scaling relationship between OER and CER

Having seen that the thickness of (101)-oriented RuO₂ films can impact binding to *O as well as the OER activity and its pH dependence, we next consider activity for CER as well. The competitive rates of OER and CER in acidic solution is typically considered bound by scaling relations between the *O (*OOH) and *OCI intermediates ⁵⁰, with RuO₂ highly active for both reactions without a means to control selectivity between them ¹⁶. As in alkaline solutions, OER activity in 0.1 M H₂SO₄ decreases with increasing film thickness (Figure 3). Upon addition of KCI to the electrolyte, exponential oxidative current is observed starting at potentials 0.1-0.2 V below OER onset, attributed to CER with its facile 2e⁻ kinetics ^{50,51}, although at higher potentials (e.g. 1.6 V vs RHE) literature notes that both CER and OER co-occur on RuO₂ ⁵². Notably, addition of 100 mM KCI results in comparably high net current for both thicknesses (with CVs for other concentrations of KCI shown in Figure S10). This suggests the relaxation via defect formation/faceting of the thicker film results in greater selectivity towards CER over OER at low overpotentials. For both thin and thick RuO₂, we observe a reaction order increasing with

applied potential from ~1.2 to ~1.9 (Figure S11) with respect to [Cl⁻], where reaction orders between 1 and 2 were rationalized by Kuo et al. to arise from potential-dependent *OCl coverage over and above the chloride concentration dependence ⁵³. Thus, the increased selectivity on thicker RuO₂ (101) may arise from decoupling binding of *OCl and *O on the surface ⁵⁴, otherwise predicted to increase linearly with one another on pristine (110) surfaces ¹⁶. Breaking such scaling relations could result from the presence of multiple active sites on relaxed surfaces, unique local coordination and H-binding, or faceting, where different facets have been predicted to have a range of CER selectivity ²⁷. Identifying such physical origins is the focus of ongoing work in our lab, as these results suggest defects may offer new opportunities in tailoring selectivity for oxidative reactions.

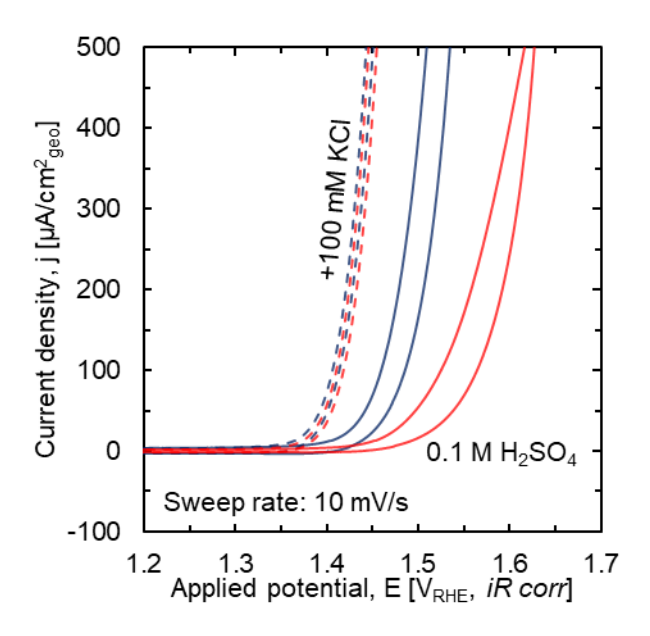


Figure 3: CV trends for 8 nm (blue) and 48 nm (red) RuO_2/r - Al_2O_3 (101) in N_2 saturated 0.1 M H_2SO_4 (OER only, solid lines) and in 0.1 M H_2SO_4 + 100 mM KCl (CER+OER, dashed lines). Comparable CER activity but distinct OER activity suggests strain relaxation via defect formation/faceting can break adsorbate scaling relations.

4. Conclusions

In this study, we report a thickness-dependent OER activity for (101)-oriented RuO₂ epitaxial films grown by SS-MOMBE. Increasing thickness of these films has been linked to strain relaxation and surface faceting via STEM ³³. Despite films behaving as metals with comparable charge transfer resistance, the OER activity decreased with increasing thickness, attributed to increased strain relaxation via defect formation and faceting. This decrease was commensurate with stronger binding of *O to the active sites for increasing film thickness, while binding of *OH remained comparable. The OER activity of thicker films increased with pH, observed previously for thick PLD-grown films (e.g. 25 nm) ⁴⁸, whereas the thinner more active films studied here (e.g. 8 nm) demonstrated pH independent behavior, indicating mechanistic differences stemming from the nature of the active site induced by strain or its relaxation. Thin RuO₂ with

residual strain is also more active for OER in acid than its thicker, relaxed counterpart, but the films have comparable CER activity in the presence of chloride salts. These findings indicate that strain relaxation and faceting may provide a unique handle to tailor not only activity but also mechanism and selectivity among competitive oxidation reactions.

Data availability

The raw and processed data required associated with the main text are available to download from 10.17632/f9zhbnstht.2. Additional data that support the findings of this study are available from the corresponding author upon reasonable request.

CRediT authorship contribution statement

Prajwal Adiga: Methodology, Investigation, Formal Analysis, Writing – Original Draft, Visualization **Dr. William Nunn:** Resources, Writing – Review and Editing **Cindy Wong:** Investigation, Writing – Review and Editing **Anusha K. Manjeshwar:** Resources, Writing – Review and Editing **Dr. Bharat Jalan:** Conceptualization, Resources, Writing – Review and Editing, Supervision, Funding acquisition **Dr. Kelsey A. Stoerzinger:** Conceptualization, Methodology, Resources, Writing – Review and Editing, Supervision, Funding acquisition

Declaration of competing interest

The authors declare that they have no known competing financial interests or personal relationships that could have appeared to influence the work reported in this paper.

Acknowledgments

This material is based upon work supported by the National Science Foundation under Grant No. 2041153. P.A. acknowledges support from the Link Foundation Energy Fellowship. K.A.S. acknowledges support from Oregon State University as a Callahan Faculty Scholar. The work at the UMN was supported primarily by the National Science Foundation through the University of Minnesota MRSEC under Award Number DMR-2011401. A.K.M and W.N. acknowledge support from the U.S. DOE through DE-SC002021 and Air Force Office of Scientific Research (AFOSR) through Grants FA9550-21-1-0025, respectively. Part of this work was also carried out in the College of Science and Engineering Characterization Facility, University of Minnesota, which has received capital equipment funding from the NSF through the UMN MRSEC program. W. N. also acknowledges support from the Vannevar Bush Faculty Fellowship.

Reference

- [1] M. Carmo, D. L. Fritz, J. Mergel, D. Stolten, A comprehensive review on PEM water electrolysis, *Int. J. Hydrogen Energy* 38 (12) (2013), 4901-4934. https://doi.org/10.1016/j.ijhydene.2013.01.151.
- [2] A. Ursua, L. M. Gandia, P. Sanchis, Hydrogen Production From Water Electrolysis: Current Status and Future Trends, *Proceedings of the IEEE* 100 (2) (2012), 410-426. https://doi.org/10.1109/JPROC.2011.2156750.
- [3] K. A. Stoerzinger, L. Qiao, M. D. Biegalski, Y. Shao-Horn, Orientation-Dependent Oxygen Evolution Activities of Rutile IrO₂ and RuO₂, *The Journal of Physical Chemistry Letters* 5 (10) (2014), 1636-1641. https://doi.org/10.1021/jz500610u.
- [4] Y. Lee, J. Suntivich, K. J. May, E. E. Perry, Y. Shao-Horn, Synthesis and Activities of Rutile IrO₂ and RuO₂ Nanoparticles for Oxygen Evolution in Acid and Alkaline Solutions, *The Journal of Physical Chemistry Letters* 3 (3) (2012), 399-404. https://doi.org/10.1021/jz2016507.
- [5] I. C. Man, H.-Y. Su, F. Calle-Vallejo, H. A. Hansen, J. I. Martínez, N. G. Inoglu, J. Kitchin, T. F. Jaramillo, J. K. Nørskov, J. Rossmeisl, Universality in Oxygen Evolution Electrocatalysis on Oxide Surfaces, *ChemCatChem* 3 (7) (2011), 1159-1165. https://doi.org/10.1002/cctc.201000397.
- [6] C. C. L. McCrory, S. Jung, J. C. Peters, T. F. Jaramillo, Benchmarking Heterogeneous Electrocatalysts for the Oxygen Evolution Reaction, *J. Am. Chem. Soc.* 135 (45) (2013), 16977-16987. https://doi.org/10.1021/ja407115p.
- [7] W. Tong, M. Forster, F. Dionigi, S. Dresp, R. Sadeghi Erami, P. Strasser, A. J. Cowan, P. Farràs, Electrolysis of low-grade and saline surface water, *Nature Energy* 5 (5) (2020), 367-377. https://doi.org/10.1038/s41560-020-0550-8.
- [8] R. K. B. Karlsson, and A. Cornell, Selectivity between Oxygen and Chlorine Evolution in the Chlor-Alkali and Chlorate Processes, *Chem. Rev.* 116 (5) (2016), 2982-3028. https://doi.org/10.1021/acs.chemrev.5b00389.
- [9] Y. Wang, Y. Liu, D. Wiley, S. Zhao, Z. Tang, Recent advances in electrocatalytic chloride oxidation for chlorine gas production, *Journal of Materials Chemistry A* 9 (35) (2021), 18974-18993. https://doi.org/10.1039/D1TA02745J.
- [10] J. Greeley, Theoretical Heterogeneous Catalysis: Scaling Relationships and Computational Catalyst Design, *Annual Review of Chemical and Biomolecular Engineering* 7 (1) (2016), 605-635. https://doi.org/10.1146/annurev-chembioeng-080615-034413.
- [11] H. Over, Fundamental Studies of Planar Single-Crystalline Oxide Model Electrodes (RuO₂, IrO₂) for Acidic Water Splitting, *ACS Catalysis* 11 (14) (2021), 8848-8871. https://doi.org/10.1021/acscatal.1c01973.
- [12] R. R. Rao, M. J. Kolb, N. B. Halck, A. F. Pedersen, A. Mehta, H. You, K. A. Stoerzinger, Z. Feng, H. A. Hansen, H. Zhou, L. Giordano, J. Rossmeisl, T. Vegge, I. Chorkendorff, I. E. L. Stephens, Y. Shao-Horn, Towards identifying the active sites on $RuO_2(110)$ in catalyzing oxygen evolution, *Energy & Environmental Science* 10 (12) (2017), 2626-2637. https://doi.org/10.1039/C7EE02307C.
- [13] J. Rossmeisl, Z. W. Qu, H. Zhu, G. J. Kroes, J. K. Nørskov, Electrolysis of water on oxide surfaces, *J. Electroanal. Chem.* 607 (1) (2007), 83-89. https://doi.org/10.1016/j.jelechem.2006.11.008.
- [14] D.-Y. Kuo, H. Paik, J. Kloppenburg, B. Faeth, K. M. Shen, D. G. Schlom, G. Hautier, J. Suntivich, Measurements of Oxygen Electroadsorption Energies and Oxygen Evolution Reaction on RuO₂(110): A Discussion of the Sabatier Principle and Its Role in Electrocatalysis, *J. Am. Chem. Soc.* 140 (50) (2018), 17597-17605. https://doi.org/10.1021/jacs.8b09657.
- [15] H. Ooka, J. Huang, K. S. Exner, The Sabatier Principle in Electrocatalysis: Basics, Limitations, and Extensions, *Frontiers in Energy Research* 9 (2021) https://doi.org/10.3389/fenrg.2021.654460.

- [16] H. A. Hansen, I. C. Man, F. Studt, F. Abild-Pedersen, T. Bligaard, J. Rossmeisl, Electrochemical chlorine evolution at rutile oxide (110) surfaces, *PCCP* 12 (1) (2010), 283-290. https://doi.org/10.1039/B917459A.
- [17] N. B. Halck, V. Petrykin, P. Krtil, J. Rossmeisl, Beyond the volcano limitations in electrocatalysis oxygen evolution reaction, *PCCP* 16 (27) (2014), 13682-13688. https://doi.org/10.1039/C4CP00571F.
- [18] S. Divanis, A. M. Frandsen, T. Kutlusoy, J. Rossmeisl, Lifting the discrepancy between experimental results and the theoretical predictions for the catalytic activity of RuO₂(110) towards oxygen evolution reaction, *PCCP* 23 (35) (2021), 19141-19145. https://doi.org/10.1039/D1CP02999A.
- [19] C. F. Dickens, and J. K. Nørskov, A Theoretical Investigation into the Role of Surface Defects for Oxygen Evolution on RuO₂, *The Journal of Physical Chemistry C* 121 (34) (2017), 18516-18524. https://doi.org/10.1021/acs.jpcc.7b03481.
- [20] Z. L. Zhao, Q. Wang, X. Huang, Q. Feng, S. Gu, Z. Zhang, H. Xu, L. Zeng, M. Gu, H. Li, Boosting the oxygen evolution reaction using defect-rich ultra-thin ruthenium oxide nanosheets in acidic media, *Energy & Environmental Science* 13 (12) (2020), 5143-5151. https://doi.org/10.1039/D0EE01960G.
- [21] A. Zagalskaya, and V. Alexandrov, Role of Defects in the Interplay between Adsorbate Evolving and Lattice Oxygen Mechanisms of the Oxygen Evolution Reaction in RuO₂ and IrO₂, ACS Catalysis 10 (6) (2020), 3650-3657. https://doi.org/10.1021/acscatal.9b05544.
- [22] N. Danilovic, R. Subbaraman, K.-C. Chang, S. H. Chang, Y. J. Kang, J. Snyder, A. P. Paulikas, D. Strmcnik, Y.-T. Kim, D. Myers, V. R. Stamenkovic, N. M. Markovic, Activity—Stability Trends for the Oxygen Evolution Reaction on Monometallic Oxides in Acidic Environments, *The Journal of Physical Chemistry Letters* 5 (14) (2014), 2474-2478. https://doi.org/10.1021/jz501061n.
- [23] A. Grimaud, O. Diaz-Morales, B. Han, W. T. Hong, Y.-L. Lee, L. Giordano, K. A. Stoerzinger, M. T. M. Koper, Y. Shao-Horn, Activating lattice oxygen redox reactions in metal oxides to catalyse oxygen evolution, *Nature Chemistry* 9 (5) (2017), 457-465. https://doi.org/10.1038/nchem.2695.
- [24] Z. Shi, Y. Wang, J. Li, X. Wang, Y. Wang, Y. Li, W. Xu, Z. Jiang, C. Liu, W. Xing, J. Ge, Confined Ir single sites with triggered lattice oxygen redox: Toward boosted and sustained water oxidation catalysis, *Joule* 5 (8) (2021), 2164-2176. https://doi.org/10.1016/j.joule.2021.05.018.
- [25] K. A. Stoerzinger, O. Diaz-Morales, M. Kolb, R. R. Rao, R. Frydendal, L. Qiao, X. R. Wang, N. B. Halck, J. Rossmeisl, H. A. Hansen, T. Vegge, I. E. L. Stephens, M. T. M. Koper, Y. Shao-Horn, Orientation-Dependent Oxygen Evolution on RuO₂ without Lattice Exchange, *ACS Energy Letters* 2 (4) (2017), 876-881. https://doi.org/10.1021/acsenergylett.7b00135.
- [26] R. R. Rao, M. J. Kolb, L. Giordano, A. F. Pedersen, Y. Katayama, J. Hwang, A. Mehta, H. You, J. R. Lunger, H. Zhou, N. B. Halck, T. Vegge, I. Chorkendorff, I. E. L. Stephens, Y. Shao-Horn, Operando identification of site-dependent water oxidation activity on ruthenium dioxide single-crystal surfaces, *Nature Catalysis* 3 (6) (2020), 516-525. https://doi.org/10.1038/s41929-020-0457-6.
- [27] S. Saha, P. Gayen, V. K. Ramani, Facet-dependent Chlorine and Oxygen Evolution Selectivity on RuO₂: An Ab initio Atomistic Thermodynamic Study, *ChemCatChem* 12 (19) (2020), 4922-4929. https://doi.org/10.1002/cctc.202000617.
- [28] A. Khorshidi, J. Violet, J. Hashemi, A. A. Peterson, How strain can break the scaling relations of catalysis, *Nature Catalysis* 1 (4) (2018), 263-268. https://doi.org/10.1038/s41929-018-0054-0.
- [29] Z. Xu, and J. R. Kitchin, Tuning oxide activity through modification of the crystal and electronic structure: from strain to potential polymorphs, *PCCP* 17 (43) (2015), 28943-28949. https://doi.org/10.1039/C5CP04840K.
- [30] J. Hwang, Z. Feng, N. Charles, X. R. Wang, D. Lee, K. A. Stoerzinger, S. Muy, R. R. Rao, D. Lee, R. Jacobs, D. Morgan, Y. Shao-Horn, Tuning perovskite oxides by strain: Electronic structure, properties, and functions in (electro)catalysis and ferroelectricity, *Mater. Today* 31 (2019), 100-118. https://doi.org/10.1016/j.mattod.2019.03.014.

- [31] G. Buvat, M. J. Eslamibidgoli, A. H. Youssef, S. Garbarino, A. Ruediger, M. Eikerling, D. Guay, Effect of IrO₆ Octahedron Distortion on the OER Activity at (100) IrO₂ Thin Film, *ACS Catalysis* 10 (1) (2020), 806-817. https://doi.org/10.1021/acscatal.9b04347.
- [32] R. Chattot, P. Bordet, I. Martens, J. Drnec, L. Dubau, F. Maillard, Building Practical Descriptors for Defect Engineering of Electrocatalytic Materials, *ACS Catalysis* 10 (16) (2020), 9046-9056. https://doi.org/10.1021/acscatal.0c02144.
- [33] W. Nunn, S. Nair, H. Yun, A. Kamath Manjeshwar, A. Rajapitamahuni, D. Lee, K. A. Mkhoyan, B. Jalan, Solid-source metal—organic molecular beam epitaxy of epitaxial RuO₂, *APL Materials* 9 (9) (2021), 091112. https://doi.org/10.1063/5.0062726.
- [34] Y. Yao, Engineering the Electronic Structure of Single Atom Ru Sites via Compressive Strain Boosts Acidic Water Oxidation Electrocatalysis. In *Controllable Synthesis and Atomic Scale Regulation of Noble Metal Catalysts*, Yao, Y., (ed.) Springer Singapore, Singapore, 2022, pp 55-92.
- [35] Y. Wen, T. Yang, C. Cheng, X. Zhao, E. Liu, J. Yang, Engineering Ru(IV) charge density in Ru@RuO₂ core-shell electrocatalyst via tensile strain for efficient oxygen evolution in acidic media, *Chinese Journal of Catalysis* 41 (8) (2020), 1161-1167. https://doi.org/10.1016/S1872-2067(20)63543-4.
- [36] G. Meng, W. Sun, A. A. Mon, X. Wu, L. Xia, A. Han, Y. Wang, Z. Zhuang, J. Liu, D. Wang, Y. Li, Strain Regulation to Optimize the Acidic Water Oxidation Performance of Atomic-Layer IrO_x, *Adv. Mater.* 31 (37) (2019), 1903616. https://doi.org/10.1002/adma.201903616.
- [37] A. R. Akbashev, Electrocatalysis Goes Nuts, *ACS Catalysis* (2022), 4296-4301. https://doi.org/10.1021/acscatal.2c00123.
- [38] P. Adiga, and K. A. Stoerzinger, Epitaxial oxide thin films for oxygen electrocatalysis: A tutorial review, *Journal of Vacuum Science & Technology A* 40 (1) (2021), 010801. https://doi.org/10.1116/6.0001429.
- [39] K. A. Stoerzinger, W. S. Choi, H. Jeen, H. N. Lee, Y. Shao-Horn, Role of Strain and Conductivity in Oxygen Electrocatalysis on LaCoO₃ Thin Films, *The Journal of Physical Chemistry Letters* 6 (3) (2015), 487-492. https://doi.org/10.1021/jz502692a.
- [40] L. Wang, K. A. Stoerzinger, L. Chang, X. Yin, Y. Li, C. S. Tang, E. Jia, M. E. Bowden, Z. Yang, A. Abdelsamie, L. You, R. Guo, J. Chen, A. Rusydi, J. Wang, S. A. Chambers, Y. Du, Strain Effect on Oxygen Evolution Reaction Activity of Epitaxial NdNiO₃ Thin Films, *ACS Applied Materials & Interfaces* 11 (13) (2019), 12941-12947. https://doi.org/10.1021/acsami.8b21301.
- [41] Z. Fatima, D. Oka, T. Fukumura, Systematic Application of Extremely Large Strain to Rutile-Type RuO₂(100) Epitaxial Thin Films on Substrates with Large Lattice Mismatches, *Crystal Growth & Design* 21 (7) (2021), 4083-4089. https://doi.org/10.1021/acs.cgd.1c00377.
- [42] K. Lee, M. Osada, H. Y. Hwang, Y. Hikita, Oxygen Evolution Reaction Activity in IrO_x/SrIrO₃ Catalysts: Correlations between Structural Parameters and the Catalytic Activity, *The Journal of Physical Chemistry Letters* 10 (7) (2019), 1516-1522. https://doi.org/10.1021/acs.jpclett.9b00173.
- [43] C. Roy, R. R. Rao, K. A. Stoerzinger, J. Hwang, J. Rossmeisl, I. Chorkendorff, Y. Shao-Horn, I. E. L. Stephens, Trends in Activity and Dissolution on RuO₂ under Oxygen Evolution Conditions: Particles versus Well-Defined Extended Surfaces, *ACS Energy Letters* 3 (9) (2018), 2045-2051. https://doi.org/10.1021/acsenergylett.8b01178.
- [44] W. Nunn, A. K. Manjeshwar, J. Yue, A. Rajapitamahuni, T. K. Truttmann, B. Jalan, Novel synthesis approach for "stubborn" metals and metal oxides, *Proceedings of the National Academy of Sciences* 118 (32) (2021), e2105713118. https://doi.org/10.1073/pnas.2105713118.
- [45] R. R. Rao, M. J. Kolb, J. Hwang, A. F. Pedersen, A. Mehta, H. You, K. A. Stoerzinger, Z. Feng, H. Zhou, H. Bluhm, L. Giordano, I. E. L. Stephens, Y. Shao-Horn, Surface Orientation Dependent Water Dissociation on Rutile Ruthenium Dioxide, *The Journal of Physical Chemistry C* 122 (31) (2018), 17802-17811. https://doi.org/10.1021/acs.jpcc.8b04284.

- [46] D.-Y. Kuo, J. K. Kawasaki, J. N. Nelson, J. Kloppenburg, G. Hautier, K. M. Shen, D. G. Schlom, J. Suntivich, Influence of Surface Adsorption on the Oxygen Evolution Reaction on IrO₂(110), *J. Am. Chem. Soc.* 139 (9) (2017), 3473-3479. https://doi.org/10.1021/jacs.6b11932.
- [47] L. Giordano, B. Han, M. Risch, W. T. Hong, R. R. Rao, K. A. Stoerzinger, Y. Shao-Horn, pH dependence of OER activity of oxides: Current and future perspectives, *Catal. Today* 262 (2016), 2-10. https://doi.org/10.1016/j.cattod.2015.10.006.
- [48] K. A. Stoerzinger, R. R. Rao, X. R. Wang, W. T. Hong, C. M. Rouleau, Y. Shao-Horn, The Role of Ru Redox in pH-Dependent Oxygen Evolution on Rutile Ruthenium Dioxide Surfaces, *Chem* 2 (5) (2017), 668-675. https://doi.org/10.1016/j.chempr.2017.04.001.
- [49] M. E. G. Lyons, and S. Floquet, Mechanism of oxygen reactions at porous oxide electrodes. Part 2—Oxygen evolution at RuO_2 , IrO_2 and $Ir_xRu_{1-x}O_2$ electrodes in aqueous acid and alkaline solution, *PCCP* 13 (12) (2011), 5314-5335. https://doi.org/10.1039/COCP02875D.
- [50] K. S. Exner, J. Anton, T. Jacob, H. Over, Controlling Selectivity in the Chlorine Evolution Reaction over RuO₂-Based Catalysts, *Angew. Chem. Int. Ed.* 53 (41) (2014), 11032-11035. https://doi.org/10.1002/anie.201406112.
- [51] J. G. Vos, Z. Liu, F. D. Speck, N. Perini, W. Fu, S. Cherevko, M. T. M. Koper, Selectivity Trends Between Oxygen Evolution and Chlorine Evolution on Iridium-Based Double Perovskites in Acidic Media, *ACS Catalysis* 9 (9) (2019), 8561-8574. https://doi.org/10.1021/acscatal.9b01159.
- [52] S. Saha, K. Kishor, R. G. Pala, Modulating Selectivity in CER and OER through Doped RuO₂, *ECS Transactions* 85 (12) (2018), 201-213. 10.1149/08512.0201ecst.
- [53] D.-Y. Kuo, H. Paik, J. N. Nelson, K. M. Shen, D. G. Schlom, J. Suntivich, Chlorine evolution reaction electrocatalysis on $RuO_2(110)$ and $IrO_2(110)$ grown using molecular-beam epitaxy, *The Journal of Chemical Physics* 150 (4) (2019), 041726. https://doi.org/10.1063/1.5051429.
- [54] K. S. Exner, Design criteria for the competing chlorine and oxygen evolution reactions: avoid the OCl adsorbate to enhance chlorine selectivity, *PCCP* 22 (39) (2020), 22451-22458. https://doi.org/10.1039/D0CP03667F.